

Insights into fibrinogen mechanics under cyclic high-strain loading

Mayar Tarek Ibrahim,¹ Sajjad Norouzi,¹ Uma Paul,¹ Sapun H. Parekh,¹ and Pengyu Ren^{1,*}

¹Department of Biomedical Engineering, University of Texas at Austin, Austin, Texas

ABSTRACT Fibrinogen plays a central role in the physiological processes of blood coagulation and, unfortunately, ischemic stroke, where it is routinely exposed to mechanical forces. In this study, we employed atomistic molecular dynamics simulations to subject fibrinogen to three cycles of high-strain loading ($\sim 17.5\text{--}27.5\%$) and unloading, enabling us to probe its mechanical response under cyclic stress. To capture the effects of pulling direction and structural asymmetry, we simulated the two different fibrinogen molecules present in the crystallographic unit cell. Forces were applied to the γ_1 nodule of molecule 1 and the γ_2 nodule of molecule 2 in opposite directions. The simulations revealed contrasting mechanical behaviors: the γ_1 nodule exhibited greater extension with partial elasticity, whereas the β -sheet-rich γ_2 nodule showed higher resistance but sustained irreversible structural damage. After force relaxation, both molecules retained residual strain (6.52–15.62% across independent replicas), confirming partial irreversibility. Anisotropic normal mode analysis further identified localized reductions in stiffness linked to unfolding of secondary structural elements, including β -sheets and α -helices. Complementary Kelvin-Voigt modeling of the unloading curves further quantified these effects, showing progressive reductions in the effective spring constant (K_{spec}) and dashpot coefficient (C_{spec}) across cycles. The model captured the viscoelastic relaxation dynamics. Collectively, these findings demonstrate that fibrinogen's cyclic response is shaped by both intrinsic structural heterogeneity, revealing viscoelastic behavior with important implications for clot formation and stroke pathogenesis.

SIGNIFICANCE Fibrinogen is an essential clotting protein that is constantly exposed to mechanical forces in the bloodstream. Despite its importance, how fibrinogen responds to repeated mechanical stress has remained unclear. Using atomistic simulations, we show that its two terminal γ -nodules, surprisingly, respond asymmetrically: the γ_1 nodule stretches with partial recovery, while the β -sheet-rich γ_2 nodule resists deformation but accumulates irreversible damage. Across multiple loading cycles, both molecules retained residual strain, indicating incomplete reversibility. By combining structural analysis with Kelvin-Voigt viscoelastic modeling, we demonstrate how fibrinogen integrates elasticity, viscosity, and plasticity. These findings provide molecular insight into the mechanical response of the fibrinogen under high-strain cyclic loading ($\sim 17.5\text{--}27.5\%$).

INTRODUCTION

Fibrinogen is a large soluble glycoprotein composed of three pairs of polypeptide chains (A α , B β , and γ) arranged in a trinodular architecture: a central E domain connects two terminal D domains (β - and γ -nodules) (Fig. 1 a), via A α , B β , and γ -chain coiled-coil segments (1,2). Fibrinogen plays an essential role in hemostasis and wound healing (3). Upon vascular injury, fibrinogen is cleaved by the enzyme thrombin to generate fibrin monomers, which polymerize

into an insoluble fibrin network that stabilizes the formation of blood clot and initiates tissue repair (4–6). γ -Nodules play crucial roles in the fibrin polymerization process (7). In addition, fibrinogen participates in diverse physiological and pathological processes, including tumor metastasis and angiogenesis (8,9). *In vivo*, fibrinogen is exposed to a variety of mechanical forces, such as shear from blood flow, platelet contraction, and tissue deformation (10–12). These forces induce conformational changes that impact fibrinogen's mechanical properties and biological function (13). Experimental studies using atomic force microscopy and optical tweezers have demonstrated that fibrinogen and fibrin exhibit nonlinear elasticity and can undergo reversible or irreversible structural transitions depending on force magnitude and duration (14,15). In addition, computational

Submitted September 23, 2025, and accepted for publication November 11, 2025.

*Correspondence: pren@utexas.edu

Editor: Ao Ma.

<https://doi.org/10.1016/j.bpj.2025.11.017>

© 2025 Biophysical Society. Published by Elsevier Inc.

All rights are reserved, including those for text and data mining, AI training, and similar technologies.

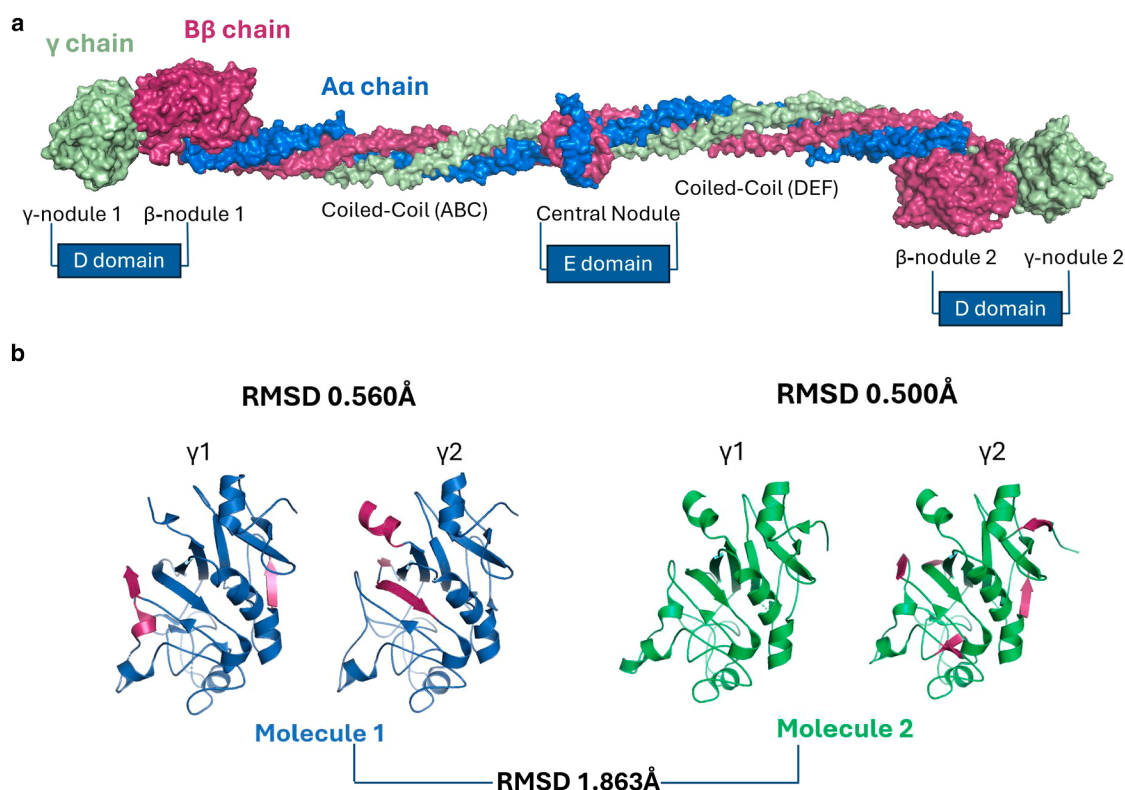


FIGURE 1 Structural organization and heterogeneity of fibrinogen γ -nodules. (a) Full-length fibrinogen crystal structure (PDB: 3GHG) showing the γ -chain (green), B β -chain (magenta), and A α -chain (blue). The molecule consists of two γ -nodules and two β -nodules located at either end, connected by coiled-coil domains (ABC and DEF) to the central E domain. (b) Structural comparison of the γ -nodules in molecule 1 (blue) and molecule 2 (green). Within each molecule, the two γ -nodules show subtle differences with RMSD values of 0.560 Å (molecule 1) and 0.500 Å (molecule 2). Across molecules, larger conformational differences are observed, with an RMSD of 1.863 Å, reflecting variability introduced by crystal packing and local structural divergence.

molecular dynamics (16) simulations were used to investigate the impact of mechanical loading on the different regions of fibrinogen (17–21). Notably, α -helices have been shown to unfold reversibly under moderate force (22,23), while β -sheets display higher stiffness but undergo abrupt, often irreversible rupture.

Despite these advances, the effect of repeated cyclic mechanical loading, resembling physiological strain from, e.g., vascular pulsatility or clot retraction, on the structural integrity of fibrinogen remains poorly understood. Moreover, existing computational studies have largely assumed symmetry between the two γ -nodules of the fibrinogen molecule (24), neglecting the structural variability present in experimentally resolved fibrinogen conformations. In reality, multiple fibrinogen variants circulate in the blood due to genetic polymorphisms and structural isoforms, with the γ -chain being the primary source of variation (25).

For example, the crystal structure of fibrinogen (PDB: 3GHG) (26) reveals two distinct protein molecules that differ noticeably in the twisting and bending of the coiled-coil domain. These molecules also vary slightly in length, containing 1914 residues in molecule 1 and 1947 in molecule 2. The 33-residue difference arises from insertions located in several regions: 12 residues in the N-terminus

of the γ -chain I (equivalent to chain C in molecule 1), 9 residues in the N-terminus of the γ -chain L (equivalent to chain F in molecule 1), and 12 residues in the C-terminus of the A α -chain J (equivalent to chain D in molecule 1). These length variations are not the focus of this study, which instead centers on pulling the C-terminal region of the γ -nodule. Structural comparison of the two crystallographic fibrinogen molecules reveals a root mean-square deviation (RMSD) of 1.863 Å (Fig. 1 b), reflecting conformational differences induced by crystal packing that capture alternative protein conformations in solution (26). In molecule 1, the γ -nodules at both ends are nearly identical in sequence, with the only distinction being the presence of an additional Gly395 in one nodule. By contrast, the γ -nodules in molecule 2 display greater variability compared with those present in molecule 1, due to extra residues located at the N-terminal region of the γ -chain. These local structural divergences are likely to influence the mechanical response of the protein. Consistent with this, secondary structure analysis reveals measurable differences, with an RMSD of 0.560 Å between the two γ -nodules in molecule 1 and 0.500 Å between the two γ -nodules in molecule 2 (Fig. 1 b).

In this study, we investigated how this structural asymmetry affects the protein mechanical response. We performed

atomistic molecular dynamics simulations of fibrinogen subjected to three cycles of high-strain (ranging between 17.5 and 27.5%) loading and unloading to investigate how pulling direction, twisting, and bending affect structural response. By applying harmonic force to one selected γ -nodule in the two distinct protein molecules ($\gamma 1$ in molecule 1 and $\gamma 2$ in molecule 2 as shown in Fig. S1), we investigated the mechanical asymmetry between them. We further characterized changes in the secondary structure using selected representative structures and assess mechanical resilience through an anisotropic network model (27) to track stiffness evolution. In addition, the Kelvin-Voigt theoretical framework was employed to extract the protein's viscoelastic properties and integrate them with the MD simulation results. Collectively, these analyses reveal that both the pulling direction and local structural differences between γ -nodules strongly influence fibrinogen's mechanical behavior. The β -sheets exhibit early and often irreversible unfolding, while α -helices show greater capacity for recovery under cyclic strain. Notably, $\gamma 1$ in molecule 1 consistently stretches more and recovers better than $\gamma 2$ in molecule 2, correlating with its greater α -helical content and fewer β -sheets. These findings suggest that fibrinogen exhibits mechanical anisotropy tied to its native structural heterogeneity, with potential implications for clot formation, elasticity, and pathological remodeling.

MATERIALS AND METHODS

System preparation

The crystal structure of single-molecule fibrinogen containing two molecules of the protein was retrieved from the Protein Data Bank (PDB: 3GHG) (28). Each fibrinogen molecule comprises three pairs of polypeptide chains (α , β , and γ) and is organized into a central E domain flanked by two terminal γ -nodules (D domains), connected by coiled-coil regions.

System preparation was performed using GROMACS v2021.3 (29,30) with the CHARMM27 all-atom force field (31). The crystal structure, composed of two distinct fibrinogen molecules, was solvated in a rectangular periodic box ($48.995 \times 15.584 \times 23.519$ nm) containing 569,914 TIP3P water atoms (32) and neutralized to physiological ionic strength by adding 31 Na^+ ions. The entire system of 1,771,181 atoms was then minimized using the steepest descent algorithm followed by equilibration in two phases: 100 ps NVT and 100 ps NPT ensembles. Long-range electrostatics were treated using the particle mesh Ewald method (33,34), and hydrogen bond lengths were constrained using the SHAKE algorithm (35), allowing a 2 fs integration time step.

Pulling simulations

Pulling simulations were carried out using the OpenMMv8.3.0 (36), specifically implementing the CustomCentroidBondForce module to apply harmonic forces. To assess the impact of structural asymmetry and pulling direction, each of the two fibrinogen molecules was subjected to pulling from opposite termini: the centroid of residue ILE394 in $\gamma 1$ of molecule 1 and the centroid of residue GLY395 in $\gamma 2$ of molecule 2 (Fig. S1). $\gamma 1$ of molecule 1 was selected because it is the only nodule in the two molecules that possesses a truncated C-terminal (terminating at ILE394 rather

than Gly395), whereas $\gamma 2$ of molecule 2 was chosen due to its higher secondary structure content, β -sheets in particular, compared with the other γ -nodule within the same molecule (Fig. 1 b).

Similar to conventional umbrella sampling, a harmonic potential with a force constant of $1000.0 \text{ kJ mol}^{-1} \text{ nm}^{-2}$ was applied to the centroid between two pulling groups (ILE394 of $\gamma 1$ in molecule 1 and Gly395 of $\gamma 2$ in molecule 2). The chosen force constant matches values used in our previous experimental and computational study (37) and was selected to achieve high strain within a short simulation time. For a macromolecular system of this size, applying large strain amplitudes is advantageous for efficiently probing mechanically relevant conformational changes under cyclic loading. Fibrinogen is a multidomain protein complex of over 1000 residues per monomer and, when simulated in explicit solvent, requires a substantially large solvation box. This leads to a high total atom count and, correspondingly, a significant computational cost. Even with GPU acceleration, our simulations achieved only ~ 1 ns per day, highlighting the scale and complexity of the system. We note that, for this reason, several prior studies have chosen to omit explicit solvent altogether to reduce computational expense (38). In this setup, the pulling force was directly proportional to the displacement.

Two independent simulations were performed in the form of three cycles of loading (1 ns each) and three cycles of unloading/relaxation (5–6 ns). These relaxation intervals were extended until no further structural recovery was observed. Unlike experimental loading-unloading systems where full recovery may occur, the protein did not return to its original conformation, indicating partial irreversibility and residual strain retention after each cycle. The final frame of each phase was extracted as the representative structure for subsequent analysis.

Strain calculation

The strain imposed on the system during pulling was computed as:

$$\text{Strain} = \frac{\Delta L}{L_0} \quad (1)$$

where ΔL is the displacement between the centroids of the two pulling residues (ILE394 in $\gamma 1$ of molecule 1 and GLY395 in $\gamma 2$ of molecule 2), and L_0 is the initial interresidue distance between the centroids of the two pulling groups. This allowed quantification of accumulated strain during each cycle in the entire system including the two distinct fibrinogen molecules.

Root mean-square fluctuation

To identify regions undergoing significant structural fluctuations during cyclic loading, root mean-square fluctuations (RMSFs) were computed for all residues using MDTraj1.9.4 (39). Comparative analysis of RMSF profiles across simulation cycles time course enabled the identification of the domains highly affected by the cyclic loading.

α -Helix/ β -sheet ratio via Ramachandran plot

Ramachandran plots were generated using MDAnalysis2.9.0 (40,41). The α -helix/ β -sheet ratio was calculated by counting the number of points falling within the angular regions' characteristic of each secondary structure. α -Helices were defined by φ angles between -120 and -30° with ψ angles from -60 to -30° , as well as φ angles between 60 and 90° with ψ angles from 0 to 60° , corresponding to the two major allowed regions for helices. β -Sheets were identified within φ angles of -180 to -45° and ψ angles of 60 – 180° , representing the canonical β -sheet region. These angular ranges were selected to capture the primary allowed conformational spaces for α -helices and β -sheets.

Ibrahim et al.

Stiffness analysis via anisotropic network model

To complement structural observations, stiffness values of the γ -nODULES were computed using the anisotropic network model (14,27) as implemented in the ProDy v2.0 package (42). ANM extends the Gaussian network model by considering directionality of motions (43,44), allowing better prediction of anisotropic fluctuations. By calculating the second derivative of the harmonic potential, ANM estimates stiffness as a function of interresidue contact geometry to estimate the collective motions of the protein. This enables identification of flexible and rigid regions, offering a quantitative analysis of the protein response to the cyclic loading/unloading.

Kelvin-Voigt theoretical model

The Kelvin-Voigt model (45) is a simple viscoelastic framework that represents a material (in this case fibrinogen) as a spring and a dashpot connected in parallel. Because the strain curves obtained from our harmonic pulling simulations closely resembled those predicted by the Kelvin-Voigt model, we employed this framework to analyze fibrinogen's mechanical response. Specifically, the model was fit to the displacement-time profiles extracted from simulation to obtain the elastic modulus E (spring constant) and viscosity η (dashpot coefficient), thereby providing insight into the physical properties of the protein under cyclic loading and unloading.

In its classical form, the Kelvin-Voigt constitutive relation under constant applied stress is expressed as:

$$\sigma(t) = E \varepsilon(t) + \eta \frac{de}{dt} \quad (2)$$

where $\sigma(t)$ is stress, $e(t)$ is strain, E is elastic modulus (spring constant), and η = viscosity (dashpot coefficient).

The corresponding force equation can be written as a function of the material properties

$$F = k_{spec} e + c_{spec} \frac{de}{dt} \quad (3)$$

where k_{spec} is spring constant, c_{spec} is the dashpot coefficient, and e is the instantaneous displacement. These parameters are related to the length and the cross-sectional area of the protein through

$$k_{spec} = E \frac{A}{L} \quad (4)$$

$$c_{spec} = \eta \frac{A}{L} \quad (5)$$

where A is cross-sectional area and L is the length of the protein.

Since our simulations employed a harmonic potential, the equations were modified to account for the constant force constant k imposed during pulling. The harmonic force is given by:

$$F = k(e_0 - e) \quad (6)$$

where e_0 is the target displacement and e is the instantaneous displacement. Substituting Eq. 6 into Eq. 3 yields:

$$c_{spec} \frac{de}{dt} + (k_{spec} + k) e = ke_0 \quad (7)$$

During the loading phase, the evolution of displacement follows:

$$\frac{de}{dt} = - \frac{(k_{spec} + k)}{c_{spec}} e + \frac{k}{c_{spec}} e_0 \quad (8)$$

During unloading (when e_0 is removed), this reduces to:

$$\frac{de}{dt} = - \frac{k_{spec}}{c_{spec}} e. \quad (9)$$

By fitting displacement-time curves to the Kelvin-Voigt formulation, the slope corresponds to $-\lambda$, where λ_{load} is $\frac{(k_{spec} + k)}{c_{spec}}$ and λ_{unload} is $\frac{k_{spec}}{c_{spec}}$ and the intercept b in during loading is $\frac{k}{c_{spec}} e_0$.

Thus, the harmonic form of Kelvin-Voigt model can be represented by the following equation

$$\frac{de}{dt} = - \lambda e + b. \quad (10)$$

The material-specific parameters are then recovered as:

$$k_{spec} = k \frac{\lambda_{unload}}{\lambda_{load} - \lambda_{unload}} \quad (11)$$

$$c_{spec} = \frac{k_{spec}}{\lambda_{unload}}. \quad (12)$$

RESULTS AND DISCUSSION

Cyclic loading reveals irreversible structural changes and asymmetric behavior between γ -nODULES

To investigate the structural response of fibrinogen to mechanical stress, $\gamma 1$ in molecule 1 and $\gamma 2$ in molecule 2 were subjected to three successive cycles of pulling and relaxation using a harmonic restraint with a force constant of 1000 kJ/mol nm² (Fig. 2). Each pulling phase (pull 1–pull 3) resulted in a sharp increase in strain within the first 100 ps, followed by a plateau. In pull 1, the strain measured between the centroids of the two pulling residues in the two distinct fibrinogen molecules ($\gamma 1$ of molecule 1 and $\gamma 2$ of molecule 2) reached a maximum of 17.5% in replica 1. The final frame was selected as the representative structure for this pulling phase. During relax 1, the strain initially decreased, but a late rise was observed after 6 ns time frame, thus the last frame at the 6 ns mark was used as representation for this phase (relax 1). Despite relaxation, ~6.5% strain was retained, indicating partial irreversibility. In pull 2, the strain increased again, reaching ~27.5%, incorporating residual strain from pull 1. Similar stabilization occurred after 100 ps, and the final frame was selected. Relax 2 allowed partial recovery, and the final 5 ns frame was used for analysis. In pull 3, the strain rose more slowly and peaked around 22.5%, suggesting the system retained a strain from prior cycles. Relax 3 revealed differential recovery: replica 1 regained compactness (retained a strain percent of 6.54%), whereas replica 2 did not (retained a strain percent of 15.62%), implying structural deformation. The strain response varied across the three cycles, reflecting

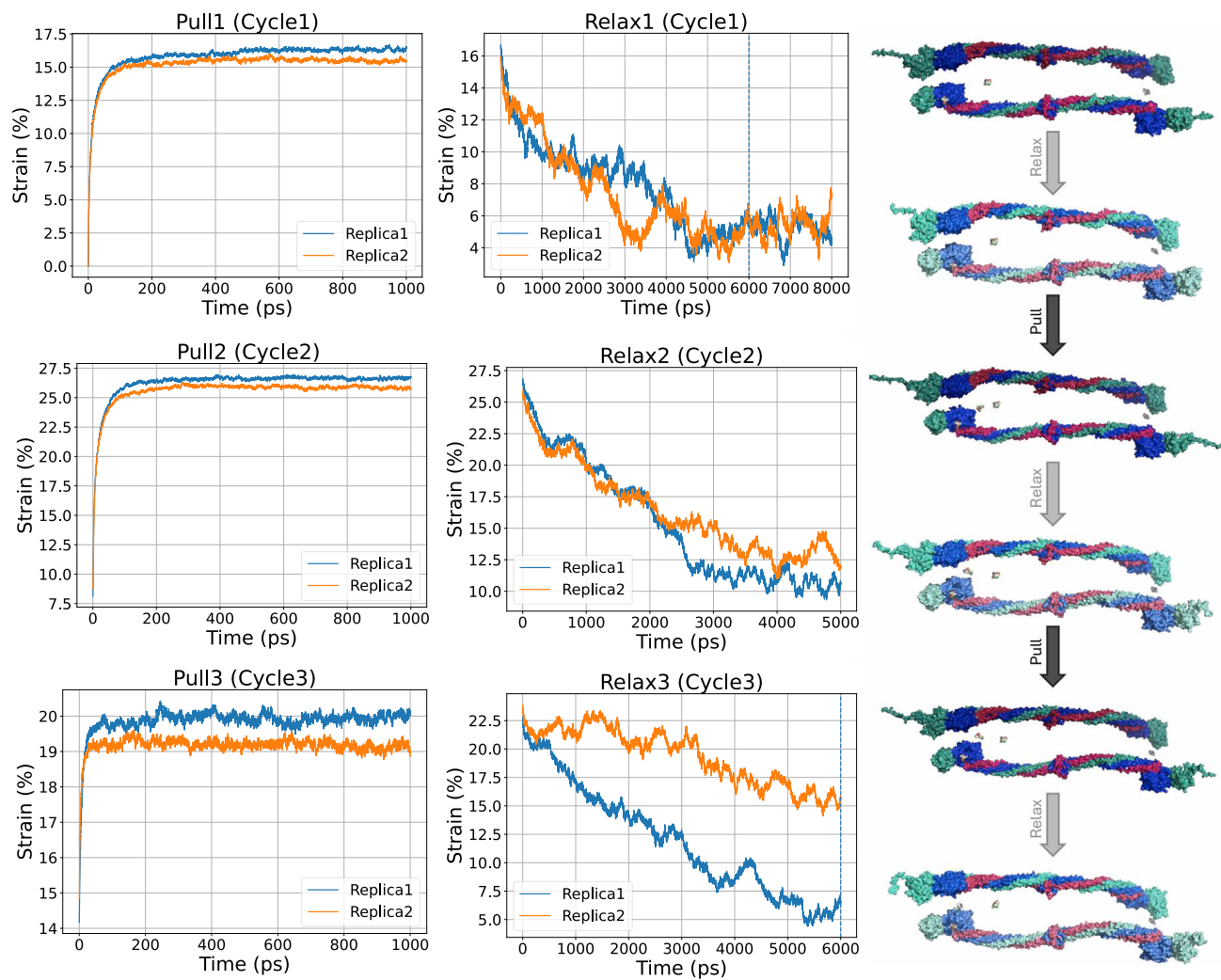


FIGURE 2 Two independent replicas of three rounds of applying harmonic potential for 1 ns on γ_1 in molecule 1 and γ_2 in molecule 2 followed by three rounds of unloading allowing the protein to relax for 8 ns in cycle 1, 5 ns in cycle 2, and 6 ns in cycle 3 (left). Selected representative structures for each cycle.

changes in the protein's mechanical resistance. During the first cycle, the protein resisted deformation, reaching a maximum strain of $\sim 17.5\%$. By the second and third cycles, higher strain levels of 27.5 and 22.5% were observed, suggesting a progressive loss of resistance to pulling forces and resulting in structural deformation.

Qualitative inspection of representative structures (Fig. 2) showed distinct responses between γ_1 and γ_2 . In pull 1, γ_1 in molecule 1 exhibited greater extension than γ_2 in molecule 2. Interestingly, γ_2 retained more compactness during relax 1. Similar trends persisted in pull 2 and relax 2, where γ_2 demonstrated greater structural recovery. By pull 3, both γ -nodules showed reduced extension capacity and, during relax 3, both exhibited curled structures indicating irreversible damage and loss of elasticity. These differences in strain accumulation and relaxation behavior between the two γ -nodules support the hypothesis of structural asymmetry in fibrinogen. The unequal mechanical responses between

γ_1 and γ_2 prompted further investigation through RMSF analysis to localize regions of high flexibility and deformation.

Structural changes trigger altered behavior

γ -Nodules and coiled-coil domains are most susceptible to cyclic pulling-induced fluctuations

To evaluate the localized structural response of fibrinogen to repeated high-strain loading, RMSF analyses were conducted across three pulling cycles. These calculations allowed the identification of regions that change under cyclic high-strain mechanical loading.

In pull 1, the γ_1 nodule in molecule 1 (residue index 696–956, highlighted in blue in Fig. 3 a) exhibited elevated fluctuations, with RMSF values ranging from 0.4 to 0.6 nm. This region was directly subjected to the applied pulling

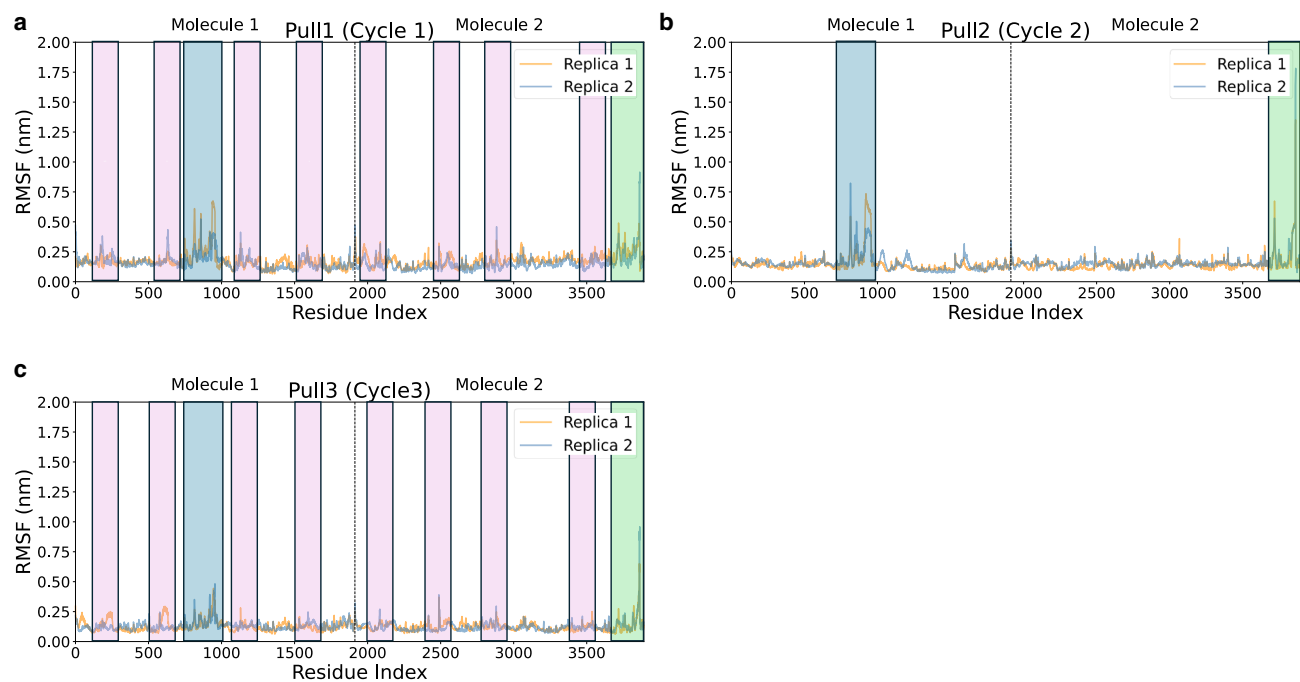


FIGURE 3 RMSF profiles reveal the fluctuations of different regions under cyclic pulling for both fibrinogen copies. The highest fluctuations are consistently observed at the pulling sites: γ_1 of molecule 1 (highlighted in blue) and γ_2 of molecule 2 (highlighted in green). Moderate fluctuations are also detected in the coiled-coil domains (highlighted in purple), particularly during pull 1. (a) Cycle 1 of pulling (Pull1). (b) Cycle 2 of pulling (Pull2). Fluctuations in the coiled-coil structure were minimal and therefore not highlighted in purple. (c) Cycle 3 of pulling (Pull3).

force. In addition, the γ_2 nodule in molecule 2 (residue index 3599–3860, highlighted in green in Fig. 3 a) also showed increased RMSF values (up to 0.8 nm). In pull 2, the asymmetry in response became more pronounced. γ_1 (molecule 1) continued to fluctuate within a range of 0.25–0.75 nm, while γ_2 (molecule 2) experienced markedly higher fluctuations, reaching 1.75 nm. This sharp increase indicates severe local instability or partial unfolding of the γ_2 nodule during this cycle. In pull 3, the trend persisted: γ_2 showed fluctuations of up to 1.0 nm, whereas γ_1 remained more stable (maximum RMSF \approx 0.5 nm).

In addition to the γ -nodules, the coiled-coil domains, specifically regions ABC (residue indices 20–174, 193–314, and 583–696 in molecule 1; 1935–2089, 2108–2229, and 2508–2621 in molecule 2) and DEF (residue indices 976–1130, 1149–1270, 1539–1652 in molecule 1; 2901–3067, 3086–3207, and 3485–3598 in copy 2) also exhibited moderate fluctuations, highlighted in purple. These helically structured linkers experienced RMSF values between 0.2 and 0.4 nm during pull 1, consistent with their role as elastic but mechanically responsive connectors. Interestingly, these coiled-coil regions were less responsive in pull 2 and pull 3, with fluctuations decreasing to \sim 0.2 nm or less, suggesting that initial strain absorption and unfolding were more dominant in the earlier stages of cyclic loading.

Taken together, the RMSF profiles across the pulling cycles confirm that γ -nodules are the primary sites of mechanical deformation, while coiled-coil domains act as

intermediate dampeners, absorbing part of the applied force without undergoing extensive unfolding. The progressive loss of structural stability in γ_2 , despite its relatively low extension (Fig. 2), emphasizes the importance of local secondary structure (notably β -sheets) in defining regional mechanical fragility under cyclic loading.

Asymmetric extension: γ_1 experiences higher strain than γ_2

As γ -nodules were found to be the most affected regions by the pulling forces, as revealed by the RMSF profiles (Fig. 3), it was essential to investigate the corresponding structural changes at the molecular level. This was achieved by analyzing the changes in the secondary structures in the selected representative structures.

In pull 1, γ_1 experienced significant structural disruption, with the loss of four β -sheets (Gly188–197, Phe215–Leu218, Ala279–Gly284, and Lys380–Pro386) and two α -helices (Ala289–Asp291 and Phe389–Thr393) (Fig. 4). In relax 1, none of the disrupted β -sheets recovered their structure, highlighting the potential irreversible nature of β -sheet unfolding. However, the α -helix Lys356–Ser358 formed during this relaxation phase, notably matching a native α -helix observed in γ_1 in molecule 2. In pull 2, this newly formed α -helix unfolded again, along with further disruption of the Ala279–Gly284 β -sheet. In relax 2, the β -sheet originally spanning Ala245–Ala263 became fragmented into two separate strands (Ala245–Asp252 and Gly255–Ala263), indicating further deformation of the secondary structure. In

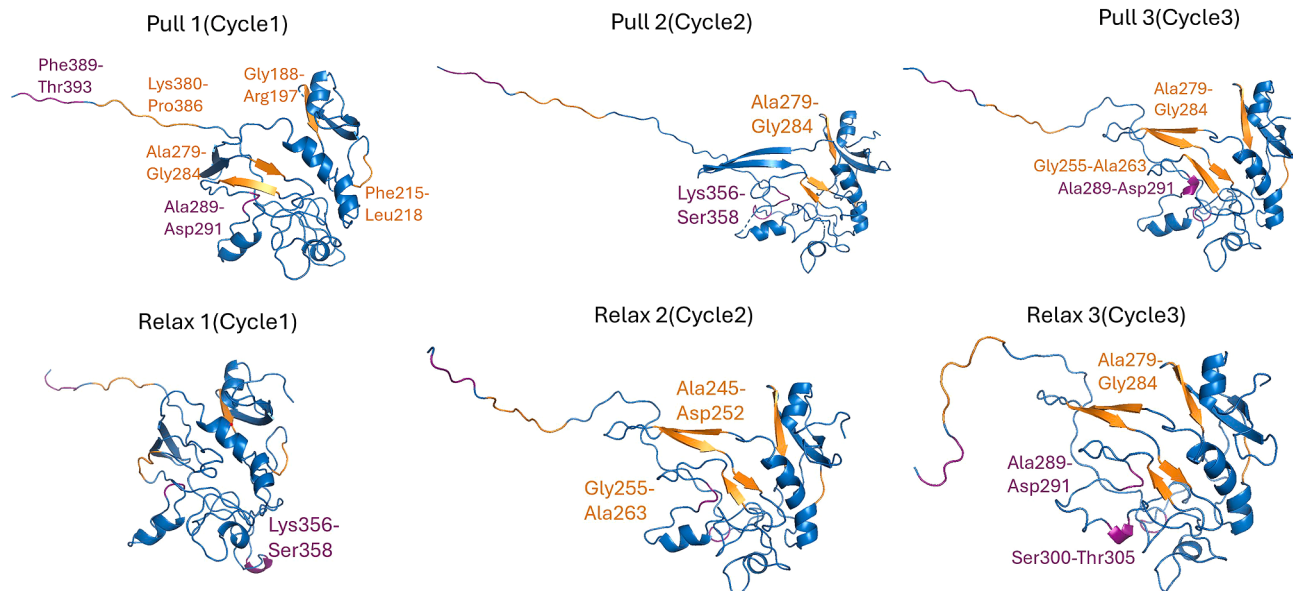


FIGURE 4 The impact of the cyclic loading and unloading on the structural changes in $\gamma 1$ in molecule 1 of the single-molecule fibrinogen. Changes in α -helices are represented in purple and changes in β -sheets are represented in orange. Only the affected regions are labeled in each cycle.

pull 3, partial recovery was observed; Ala289-Asp291 reformed its α -helical structure, while the Gly255-Ala263 and Ala279-Gly284 β -sheets exhibited further unfolding. This cycle exhibited minimal additional secondary structure loss, consistent with the reduced RMSF values observed in this phase (Fig. 3). In relax 3, a new α -helix (Ser300-Thr305) emerged, while Ala289-Asp291 was again disrupted and the Ala279-Gly284 β -sheet was lost. The reduced extent of structural change during pull 3 likely reflects the

lower strain applied, as the system had already absorbed significant deformation during pull 1 and pull 2.

In contrast, $\gamma 2$ underwent more severe structural degradation (Fig. 5). Seven β -sheets were lost during pull 1 (Gly188-Arg197, Phe215-Leu218, Tyr280-Gly283, Tyr244-Leu246, Gln311-Ser313, Trp334-Met336, and Lys380-Pro386), along with two α -helices (Phe389-Gly395 and Pro269-Lys273). Interestingly, a short α -helix (Lys356-Ser358), native to $\gamma 2$ in copy 2, formed transiently in $\gamma 1$ but was lost during relax

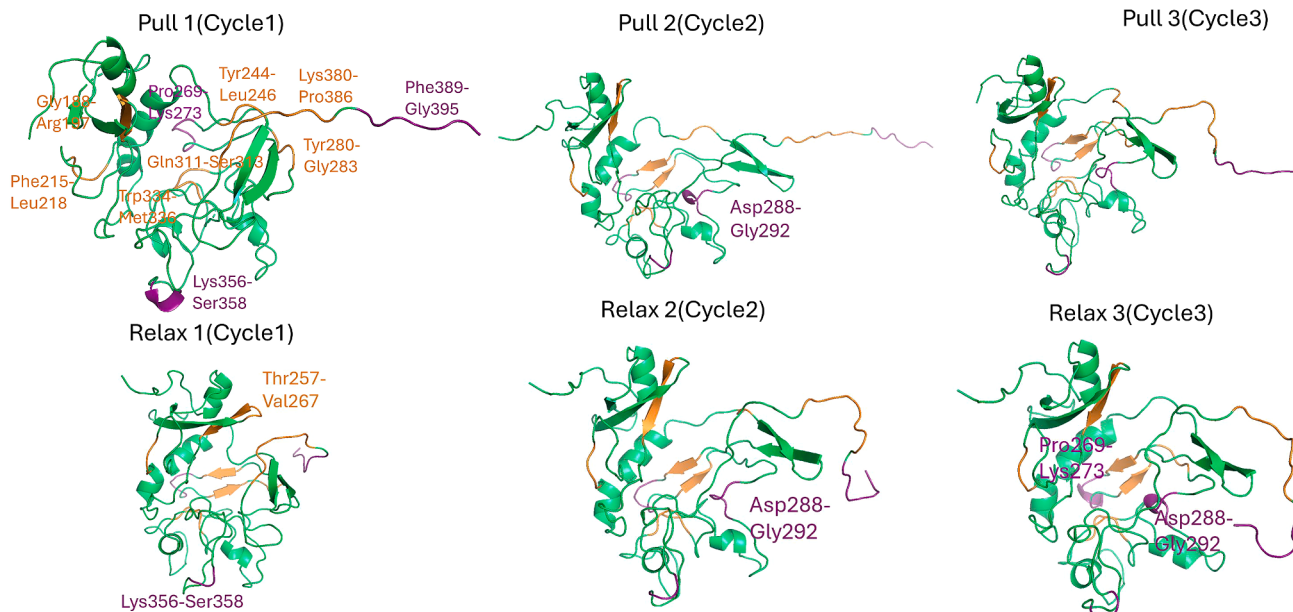


FIGURE 5 The impact of the cyclic loading and unloading on the structural changes in $\gamma 2$ of molecule 2 of the protein. Changes in α -helices are represented in purple and changes in β -sheets are represented in orange. Only the affected regions are labeled in each cycle.

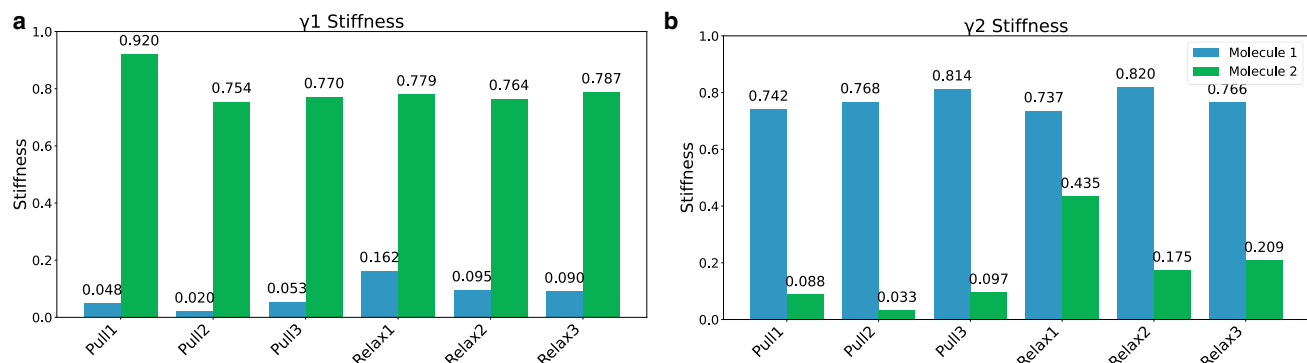


FIGURE 6 Stiffness analysis highlights the effects of pulling direction and structural asymmetry. (a) Stiffness values of γ_1 in the two distinct fibrinogen molecules (molecule 1 shown in blue and molecule 2 in green) across three cycles of loading and unloading when γ_1 in molecule 1 is the pulling point. (b) Stiffness values of γ_2 in both copies during the same simulation protocol when γ_2 in copy 2 is subjected to pulling.

1, alongside unfolding of Thr257-Val267. In pull 2, Asp288-Gly292 formed a short α -helix that again unfolded in relax 2. Pull 3 did not show further significant unfolding, while in relax 3 some recovery of α -helices was noted, specifically Pro269-Lys273 and Asp288-Gly292.

In summary, γ_1 (molecule 1) stretched more extensively but preserved much of its secondary structure, especially α -helices, due to their ability to reversibly unfold and refold. γ_2 (molecule 2), richer in β -sheets, suffered greater irreversible damage early in the simulation and resisted further extension, thereby preserving its overall compactness (Fig. 2). This structural degradation explains the elevated RMSF values observed in γ_2 across all three pulling cycles (Fig. 3). The greater abundance of β -sheets in γ_2 made it more susceptible to early structural unfolding compared with γ_1 . These observations reflect the distinct mechanical behavior of β -sheets and α -helices. β -Sheets, while initially stiff, unfold irreversibly under tension due to abrupt hydrogen bond rupture and poor realignment, making recovery unlikely (46). α -Helices (23), in contrast, display a more elastic and reversible behavior, able to unwind under low to moderate force and reform during relaxation phases. This behavior is consistent with prior single-molecule pulling simulations, where α -helices act like entropic springs and β -sheets exhibit brittle failure (23,46).

The differences in α -helix and β -sheet populations were further quantified using Ramachandran plots of the γ -nodules from representative structures subjected to cyclic pulling (Fig. S2). To assess secondary structure balance, the α -helix/ β -sheet ratio was calculated (Fig. S3). Across all three pulling cycles, γ_1 in molecule 1 consistently exhibited a higher α/β ratio compared with γ_2 in molecule 2 (pull 1, 0.352 vs. 0.348; pull 2, 0.362 vs. 0.357; pull 3, 0.414 vs. 0.379). These results confirm that γ_1 , enriched in α -helices, responds to cyclic loading with greater extensibility, whereas γ_2 , containing more β -sheets, is less resilient. This structural asymmetry underlies the differential mechanical response of the two γ -nodules.

Stiffness analysis of γ -nodules under cyclic loading

Stiffness calculations of the γ -nodules were performed using the anisotropic network model (14) to quantify the mechanical impact of repeated cyclic loading and structural asymmetry between the two fibrinogen molecules. These calculations, based on the selected representative structures extracted at the end of each pulling and relaxation phase, provide insight into the local mechanical resilience of each γ -nodule under directional force application.

When γ_1 in molecule 1 was directly subjected to pulling forces (Fig. 6 a), its stiffness dropped dramatically 0.048. This sharp decrease indicates that γ_1 undergoes significant structural softening upon force application. In contrast, molecule 2, which was not directly pulled in this condition, maintained consistently high γ_1 stiffness across all three cycles. This mechanical preservation highlights how pulling direction strongly results in localized deformation. Similarly, when γ_2 in molecule 2 was pulled (Fig. 6 b), its stiffness was markedly reduced to 0.088 in pull, whereas γ_2 in molecule 1, not subjected to direct pulling, retained higher stiffness throughout. Notably, the lowest stiffness values for the pulled nodules in both panels occurred in pull 2, corresponding to the phase with the highest recorded strain and most extensive secondary structure disruption (particularly β -sheet unfolding). This correlation supports the conclusion that stiffness loss is closely tied to irreversible structural deformation. Interestingly, in pull 3, stiffness partially recovered for both γ -nodules. This trend may reflect reduced strain accumulation in this final pulling cycle, as well as the reformation of some α -helices. In the relaxation phases, stiffness of the nonpulled nodules remained relatively stable, while the pulled nodules showed modest recovery; most notably in γ_2 , whose stiffness rose from 0.033 in pull 2 to 0.209 in relax 3.

Together, the mechanical response is asymmetric between γ_1 and γ_2 , with γ_2 exhibiting generally higher stiffness, likely due to its greater β -sheet content. These

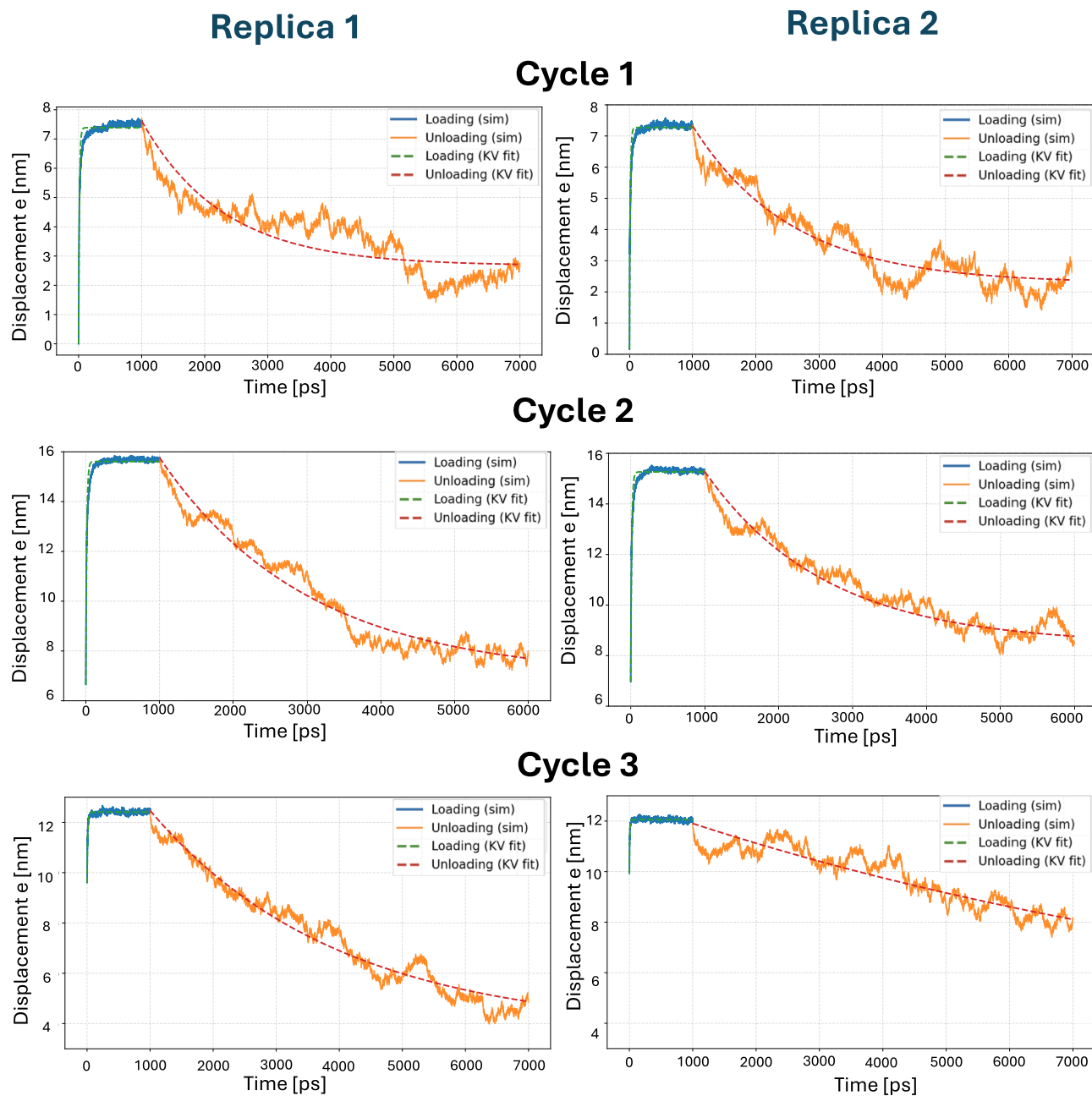


FIGURE 7 Cyclic loading-unloading simulations of fibrinogen analyzed using the Kelvin-Voigt (KV) viscoelastic model. Displacement-time curves are shown for three consecutive cycles (cycles 1–3) in replica 1 (*left*) and replica 2. Blue curves represent loading under harmonic pulling, while orange curves represent unloading. Dashed green and red lines correspond to KV fits for loading and unloading phases, respectively.

insights highlight the importance of considering both pulling direction and local structural composition when evaluating protein mechanical behavior under physiological or pathological forces to the pulling force. This asymmetric behavior is physiologically meaningful: during clot formation and subsequent exposure to blood flow, fibrin fibers experience repeated tensile and shear stresses. In this context, γ_2 likely functions as a mechanical stabilizer, maintaining fiber integrity and preventing premature overextension, whereas γ_1 may act as a mechanical

buffer, absorbing strain and allowing the clot to remain extensible without rupturing. Such division of mechanical roles could help the fibrin network balance ductility and strength, ensuring that clots are both resilient enough to withstand hemodynamic forces and sufficiently compliant to deform during vessel movement and remodeling. This highlights the broader principle that local secondary structure composition is a key determinant of mechanical performance in protein networks operating under physiological load.

Ibrahim et al.

Kelvin-Voigt theoretical model

The cyclic loading-unloading simulations were analyzed using the Kelvin-Voigt viscoelastic model to characterize the relaxation dynamics of fibrinogen under repeated strain (Fig. 7). During each cycle, the loading phase showed an almost instantaneous rise in displacement as the harmonic potential was applied, reflecting the direct impact of the force on the γ -nODULES. In contrast, the unloading phases displayed a gradual exponential-like decay in displacement, which was well approximated by the Kelvin-Voigt fits. The model successfully reproduced the relaxation slopes and corresponding time constants (λ), thereby providing estimates of the effective elastic modulus and viscosity. In all cycles, residual strain persisted at the end of unloading, and this irreversibility accumulated over successive cycles, indicative of structural damage and irreversible deformation that the Kelvin-Voigt model captures.

The progressive reduction in peak displacement from cycle 1 to cycle 3 highlights the cumulative weakening of the fibrinogen structure under repeated stress. This is consistent with irreversible unfolding of β -sheet motifs, which fail to refold upon unloading, in contrast to α -helical segments that display partial recovery. Replica 1 and replica 2 both followed this general viscoelastic-plastic trend, although replica 2 exhibited slightly slower relaxation.

Kelvin-Voigt fitting of the cyclic loading-unloading simulations revealed progressive changes in the viscoelastic properties of fibrinogen (Table S1). During the first cycle, both replicas exhibited relatively high stiffness ($K_{\text{spec}} = 10.06$ and $7.85 \text{ kJ mol}^{-1} \text{ nm}^{-2}$) and large dashpot coefficients ($\sim 12,000$ – $13,000 \text{ kJ mol}^{-1} \text{ nm}^{-2} \text{ ps}$), reflecting the intact structure's ability to resist deformation. By the second cycle, replica 1 displayed a noticeable reduction in stiffness ($6.34 \text{ kJ mol}^{-1} \text{ nm}^{-2}$) while replica 2 remained largely unchanged ($8.01 \text{ kJ mol}^{-1} \text{ nm}^{-2}$), although both retained high viscous damping. In the third cycle, both replicas underwent dramatic softening, with replica 1 and replica 2 decreasing to 3.39 and $0.57 \text{ kJ mol}^{-1} \text{ nm}^{-2}$, respectively. Viscosity also declined significantly ($C_{\text{spec}} \approx 6400$ – $10,000$), indicating diminished capacity for deformation resistance. The deviations in the spring constants and dashpot coefficients observed between the two independent replicas across cycles can be attributed to differences in retained strain (Fig. 2). Replica 2 exhibited a higher residual strain during relax 3 (cycle 3), which corresponded to a greater reduction in both the spring constant and the dashpot coefficient. These results suggest that, while the overall mechanical trends of the two replicas are consistent, the absolute values diverge depending on the extent of strain retained, reflecting variability in fibrinogen's response under different loading conditions.

Compared with elastin and fibrin fibers (15,47–49) (Table S2), fibrinogen is less resilient, showing irreversible

softening after repeated cycles. Compared with collagen (50,51), it is softer and more dissipative, allowing it to absorb energy but at the cost of plastic deformation. Its behavior most closely resembles viscoelastic synthetic polymers or cytoskeletal networks (52), which also exhibit creep, residual strain, and cycle-dependent weakening. This highlights fibrinogen's unique mechanical role: a sacrificial protein optimized for energy dissipation and irreversible remodeling during clot formation, rather than for permanent load-bearing like collagen.

CONCLUSION

The mechanical response of fibrinogen is shaped by structural variability among circulating variants, driven by genetic polymorphisms and isoforms, with the γ -chain as a major source of heterogeneity. Our simulations highlight a striking asymmetry between the $\gamma 1$ and $\gamma 2$ nodules of the two fibrinogen molecules: $\gamma 1$ undergoes greater extension with partial recovery, whereas the β -sheet-rich $\gamma 2$ resists deformation but sustains irreversible damage. This directional dependence underscores that fibrinogen's mechanics differ across domains, with β -sheets being more susceptible to disruption while α -helices retain greater resilience. Kelvin-Voigt modeling quantified these differences, revealing progressive reductions in both spring constant (K_{spec}) and dashpot coefficient (C_{spec}) across cycles. The model captured viscoelastic relaxation and residual strain, demonstrating that fibrinogen's cyclic mechanics can be effectively described within a viscoelastic framework.

DATA AND CODE AVAILABILITY

- The crystal structure including the two distinct fibrinogen molecules was retrieved from the Protein Data Bank (PDB: 3GHG).
- All data and simulation trajectories supporting the findings of this study are available from the corresponding author upon request.

ACKNOWLEDGMENTS

This research was funded by the National Institutes of Health (grant no. R01GM106137), the Welch Foundation (grant no. F-2120), and the Cancer Prevention and Research Institute of Texas (grant no. RP210088). We further acknowledge support from the National Science Foundation through grant 2105175, and the Welch Foundation through grant F-2008-20220331.

AUTHOR CONTRIBUTIONS

Conceptualization, M.T.I. and P.R.; methodology, M.T.I. and P.R.; validation, M.T.I. and P.R.; formal analysis, M.T.I. and P.R.; investigation, M.T.I. and P.R.; resources, P.R. and S.H.P.; data curation, M.T.I. and S.N.; writing – original draft, M.T.I. and P.R.; writing – review & editing, M.T.I., S.N., S.H.P., and P.R.; visualization, M.T.I. and U.P.; supervision, P.R. and S.H.P.; funding acquisition, P.R. and S.H.P. All authors have read and agreed to the published version of the manuscript.

DECLARATION OF INTERESTS

The authors declare no conflict of interest.

DECLARATION OF GENERATIVE AI AND AI-ASSISTED TECHNOLOGIES IN THE WRITING PROCESS

ChatGPT-5 was used to derive the strain response under harmonic stress using the Kelvin-Voigt viscoelastic model.

SUPPORTING MATERIAL

Supporting material can be found online at <https://doi.org/10.1016/j.bpj.2025.11.017>.

REFERENCES

- Blombäck, B. 1996. Fibrinogen and fibrin–proteins with complex roles in hemostasis and thrombosis. *Clin. Hemorheol. Microcirc.* 16:383–477.
- Herrick, S., O. Blanc-Brude, ..., G. Laurent. 1999. Fibrinogen. *Int. J. Biochem. Cell Biol.* 31:741–746.
- Fuss, C., J. C. Palmaz, and E. A. Sprague. 2001. Fibrinogen: structure, function, and surface interactions. *J. Vasc. Interv. Radiol.* 12:677–682.
- Weisel, J. W. 2007. Structure of fibrin: impact on clot stability. *J. Thromb. Haemost.* 5:116–124.
- Weisel, J. W., and R. I. Litvinov. 2013. Mechanisms of fibrin polymerization and clinical implications. *Blood.* 121:1712–1719.
- Litvinov, R. I., M. Pieters, ..., J. W. Weisel. 2020. Fibrinogen and fibrin. In *Macromolecular Protein Complexes III: Structure and Function* Springer International Publishing, pp. 471–501.
- Siebenlist, K. R., M. W. Mosesson, ..., L. Stojanovic. 2005. Studies on the basis for the properties of fibrin produced from fibrinogen-containing γ' chains. *Blood.* 106:2730–2736.
- van Hinsbergh, V. W., A. Collen, and P. Koolwijk. 2001. Role of fibrin matrix in angiogenesis. *Ann. N. Y. Acad. Sci.* 936:426–437.
- Staton, C. A., N. J. Brown, and C. E. Lewis. 2003. The role of fibrinogen and related fragments in tumour angiogenesis and metastasis. *Expert Opin. Biol. Ther.* 3:1105–1120.
- Campbell, R. A., M. Aleman, ..., A. S. Wolberg. 2010. Flow profoundly influences fibrin network structure: implications for fibrin formation and clot stability in haemostasis. *Thromb. Haemost.* 104:1281–1284.
- Gersh, K. C., K. E. Edmondson, and J. W. Weisel. 2010. Flow rate and fibrin fiber alignment. *J. Thromb. Haemost.* 8:2826–2828.
- Jawerth, L., S. Muenster, and D. A. Weitz. 2013. The mechanical mechanism of platelet induced clot stiffening. *Biophys. J.* 104:150a.
- Litvinov, R. I., and J. W. Weisel. 2017. Fibrin mechanical properties and their structural origins. *Matrix Biol.* 60–61:110–123.
- Janmey, P. A., E. J. Amis, and J. D. Ferry. 1983. Rheology of fibrin clots. VI. Stress relaxation, creep, and differential dynamic modulus of fine clots in large shearing deformations. *J. Rheol.* 27:135–153.
- Liu, W., L. M. Jawerth, ..., M. Guthold. 2006. Fibrin fibers have extraordinary extensibility and elasticity. *Science.* 313:634.
- Srivastava, D. K., V. Navratna, ..., E. Gouaux. 2024. Structure of the human dopamine transporter and mechanisms of inhibition. *Nature.* 632:672–677.
- Zhmurov, A. 2011. Transition of α -helical coiled coils to β -sheets. *Structure.* 19:1515–1524.
- Zhmurov, A. 2012. Multiscale mechanics of fibrin(ogen): Molecular dynamics and coarse-grained simulations. *J. Am. Chem. Soc.* 134:20396–20403.
- Zhmurov, A., A. E. X. Brown, ..., V. Barsegov. 2011. Mechanism of fibrin (ogen) forced unfolding. *Structure.* 19:1615–1624.
- Zhmurov, A., O. Kononova, ..., J. W. Weisel. 2012. Mechanical transition from α -helical coiled coils to β -sheets in fibrin (ogen). *J. Am. Chem. Soc.* 134:20396–20402.
- Zhmurov, A., A. D. Protopopova, ..., V. Barsegov. 2018. Atomic structural models of fibrin oligomers. *Structure.* 26:857–868.e4.
- Mykuliak, V. V., M. Sikora, ..., V. P. Hytönen. 2020. Mechanical unfolding of proteins—a comparative nonequilibrium molecular dynamics study. *Biophys. J.* 119:939–949.
- Berkemeier, F., M. Bertz, ..., M. Rief. 2011. Fast-folding α -helices as reversible strain absorbers in the muscle protein myomesin. *Proc. Natl. Acad. Sci. USA.* 108:14139–14144.
- Lord, S. T. 2011. Molecular mechanisms affecting fibrin structure and stability. *Arterioscler. Thromb. Vasc. Biol.* 31:494–499.
- Weisel, J. W., and R. I. Litvinov. 2017. Fibrin formation, structure and properties. In *Fibrous Proteins: Structures and Mechanisms* Springer, pp. 405–456.
- Kollman, J. M. 2009. Crystal Structure of Human Fibrinogen. *Structure.* 17:66–76.
- Atilgan, A. R., S. R. Durell, ..., I. Bahar. 2001. Anisotropy of fluctuation dynamics of proteins with an elastic network model. *Biophys. J.* 80:505–515.
- Kollman, J. M., L. Pandi, ..., R. F. Doolittle. 2009. Crystal structure of human fibrinogen. *Biochemistry.* 48:3877–3886.
- Abraham, M. J., T. Murtola, ..., E. Lindahl. 2015. GROMACS: High performance molecular simulations through multi-level parallelism from laptops to supercomputers. *SoftwareX.* 1–2:19–25.
- Van Der Spoel, D., E. Lindahl, ..., H. J. C. Berendsen. 2005. GROMACS: fast, flexible, and free. *J. Comput. Chem.* 26:1701–1718.
- Bjelkmar, P., P. Larsson, ..., E. Lindahl. 2010. Implementation of the CHARMM force field in GROMACS: analysis of protein stability effects from correction maps, virtual interaction sites, and water models. *J. Chem. Theory Comput.* 6:459–466.
- Price, D. J., and C. L. Brooks, 3rd. 2004. A modified TIP3P water potential for simulation with Ewald summation. *J. Chem. Phys.* 121:10096–10103.
- Darden, T., D. York, and L. Pedersen. 1993. Particle mesh Ewald: An N log (N) method for Ewald sums in large systems. *J. Chem. Phys.* 98:10089–10092.
- Essmann, U., L. Perera, ..., L. G. Pedersen. 1995. A smooth particle mesh Ewald method. *J. Chem. Phys.* 103:8577–8593.
- Kräutler, V., W. F. Van Gunsteren, and P. H. Hünenberger. 2001. A fast SHAKE algorithm to solve distance constraint equations for small molecules in molecular dynamics simulations. *J. Comput. Chem.* 22:501–508.
- Eastman, P., R. Galvelis, ..., T. E. Markland. 2023. OpenMM 8: molecular dynamics simulation with machine learning potentials. *J. Phys. Chem. B.* 128:109–116.
- Norouzi, S., M. J. Lohr, ..., S. H. Parekh. 2025. Loading causes molecular damage in fibrin fibers. *Soft Matter.* 21:8334–8347.
- Yang, Z., I. Mochalkin, and R. F. Doolittle. 2000. A model of fibrin formation based on crystal structures of fibrinogen and fibrin fragments complexed with synthetic peptides. *Proc. Natl. Acad. Sci. USA.* 97:14156–14161.
- McGibbon, R. T., K. A. Beauchamp, ..., V. S. Pande. 2015. MDTraj: a modern open library for the analysis of molecular dynamics trajectories. *Biophys. J.* 109:1528–1532.
- Michaud-Agrawal, N., E. J. Denning, ..., O. Beckstein. 2011. MDA-analysis: a toolkit for the analysis of molecular dynamics simulations. *J. Comput. Chem.* 32:2319–2327.

Ibrahim et al.

41. Gowers, R. J., M. Linke, ..., I. M. Kenney. 2019. MDAnalysis: A Python Package for the Rapid Analysis of Molecular Dynamics Simulations. Los Alamos National Laboratory (LANL), Los Alamos, NM (United States), pp. 2575–9752.
42. Zhang, S., J. M. Krieger, ..., I. Bahar. 2021. ProDy 2.0: increased scale and scope after 10 years of protein dynamics modelling with Python. *Bioinformatics*. 37:3657–3659.
43. Kitao, A., and N. Go. 1999. Investigating protein dynamics in collective coordinate space. *Curr. Opin. Struct. Biol.* 9:164–169.
44. Prigogine, I., and S. A. Rice. 2009. In *Proteins: A Theoretical Perspective of Dynamics, Structure, and Thermodynamics*, 71 John Wiley & Sons.
45. Serra-Aguila, A., J. M. Puigoriol-Forcada, ..., J. Menacho. 2019. Viscoelastic models revisited: characteristics and interconversion formulas for generalized Kelvin–Voigt and Maxwell models. *Acta Mech. Sin.* 35:1191–1209.
46. Brockwell, D. J., G. S. Beddard, ..., S. E. Radford. 2005. Mechanically unfolding the small, topologically simple protein L. *Biophys. J.* 89:506–519.
47. Aaron, B. B., and J. M. Gosline. 1981. Elastin as a random-network elastomer: A mechanical and optical analysis of single elastin fibers. *Biopolymers*. 20:1247–1260.
48. Sherratt, M. J. 2009. Tissue elasticity and the ageing elastic fibre. *Age*. 31:305–325.
49. Piechocka, I. K., R. G. Bacabac, ..., G. H. Koenderink. 2010. Structural hierarchy governs fibrin gel mechanics. *Biophys. J.* 98:2281–2289.
50. Fratzl, P. 2008. Collagen: structure and mechanics, an introduction. In *Collagen: Structure and Mechanics* Springer, pp. 1–13.
51. Gautieri, A., M. J. Buehler, and A. Redaelli. 2009. Deformation rate controls elasticity and unfolding pathway of single tropocollagen molecules. *J. Mech. Behav. Biomed. Mater.* 2:130–137.
52. Ward, M., and J. Sweeney. 2012. The Mechanical Properties of Polymers: General Considerations. In *Mechanical Properties of Solid Polymers* John Wiley & Sons, Inc, pp. 19–29.